Materials Horizons

Accepted Manuscript
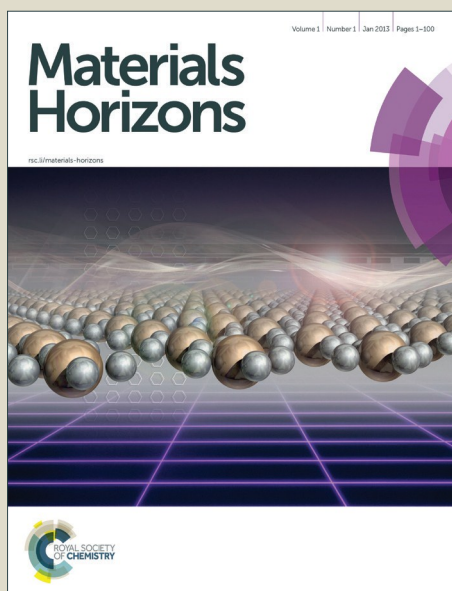
ROYAL SOCIETY OF CHEMISTRY

rsc.li/materials-horizons

Journal Name

COMMUNICATION

Multi-functional Silicone Stamps for Reactive Release Agent Transfer in UV Roll-to-Roll Nanoimprinting

J. J. Dumond,*[a] H. Y. Low,*[b] H.P. Lee,[c] and J. Y. H. Fuh[c]

A study is presented on the transfer of low surface tension reactive monomers such as monomethacryloxypropyl-terminated poly-dimtheylsiloxane (mPDMS) from a host bi-layer hard-PDMS (h-PDMS) / PDMS silicone mold to cured resin coated web surfaces in situ during UV roll-to-roll nanoimprint lithography. Here the bi-layer silicone mold plays a dual role as both a lithographic template as well as a release agent transfer vehicle, accomplishing both tasks without additional in-line processing steps. This paper is thus an early investigation into large area multi-functional silicone stamps designed especially for production of low surface energy polymer resin molds via roll-to-roll processing.

Introduction

Low and controllable surface energy in nanoimprint lithography is of critical importance in achieving a low work of adhesion between the mold and the patterning media in the imprint stack and has a direct impact on feature fidelity and process yield.[1, 2] Engineering of the mold surface energy is generally accomplished through two means: the application of anti-stick coatings,[3, 4] or fabrication of the mold entirely of intrinsically low surface energy mold materials such as fluoropolymers or silicones.[5-9] In the context of UV roll-to-roll

Conceptual Insights

Solid silicones are widely used in lithographic templating to reproduce micro- and nano-scale surface textures for a wide range of applications. Silicones are also highly permeable to and will readily absorb a large variety of non-polar fluids. With more recent advances in silicone materials chemistry, most notably the production of silicones with greater crosslink density, it is now feasible to consider exploiting both crucial aspects of silicones in the design of nanoimprint molding stamps. Here the concept of a multi-functional, bi-layer silicone stamp that can pattern UV curable resin materials as well as transfer release agent to cured resin surfaces via spontaneous molecular diffusion-based processes is introduced. Here the bi-layer silicone stamp is comprised of a thin, hard-PDMS (h-PDMS) pattern carrying layer backed by Sylgard 184 PDMS. The enhanced crosslink density of h-PDMS enables high resolution patterning as well as reduction in the swelling response to absorption of liquid monomethacryl-oxypropyl-terminated polydimethylsiloxane (mPDMS), used herein as a release agent to reduce the surface energy of UV roll-to-roll nanoimprinted

nanoimprinting as a subset to nanoimprinting generally,[10-12] specifically with regard to the roller mold or roll-mounted mold, the latter approach is often preferred due to degradation issues arising with anti-stick coatings during the UV curing and separation steps.[13]

[a.] Institute of Materials Research & Engineering (IMRE), Agency for Science, Technology & Research (A*STAR), 3 Research Link, Singapore 117602, E-mail: jdumond@gmail.com
[b.] Singapore University of Technology & Design, 8 Somapah Road, Singapore 487372, E-mail: hongyee_low@sutd.edu.sg
[c.] Mechanical Engineering Department, National University of Singapore, 9 Engineering Drive 1, Singapore 117575
†Electronic Supplementary Information (ESI) available: [details of any supplementary information available should be included here]. See DOI: 10.1039/x0xx00000x

Recently, however, interest in mass produced UV roll-to-roll nanoimprinted resin polymer molds has increased.[14-17] Resin molds produced by this means are typically negative relief replicas of the aforementioned roll mold pattern, and are fabricated into a cured resin coating deposited on a continuous, flexible plastic substrate web feed.[14] Nanolithography via resin molds is particularly important for high volume applications such as nanostructured surfaces for bio-medical devices,[18-20] light extraction structures for optoelectronics,[21-23] and anti-wetting, self-cleaning surfaces for building facades, photovoltaic panels, and signage.[24, 25] For these applications, resin polymer molds are uniquely suited as one-time-use, disposable nanolithographic templates for low cost processing. The short service lifetime of resin molds also re-opens the case for using surface modification techniques to lower the resin mold surface energy for downstream lithographic processing, as degradative processes will not affect release performance. Manipulation of the surface chemistry has several advantages over the use of intrinsically low surface energy bulk materials. First, the former allows the bulk resin formulation to be selected for application-specific properties such as high stiffness, hardness, scratch resistance and transparency. Commonly employed fluorinated or silicone-based resins generally suffer in one or more of these areas, require lengthy curing times in an inert environment making them unsuitable for high throughput roll-to-roll processing,[7, 8, 26] or are too costly for high volume manufacturing.[26] In contrast, surface chemistry modification allows for the use of widely available, fast-curing and relatively inexpensive acrylate-based resin formulations to be employed for production of resin molds. With thousands of available monomer, crosslinker and photoinitiator combinations, the resin mold properties can be adjusted easily to suit the target application.

One of the major challenges relating to surface chemistry modification to lower the surface energy of resin molds is in devising a suitable delivery mechanism. Widely used fluorinated and silicone-based, reactive chlorosilane chemistries require a densely hydroxylated surface that is not common to polymerized resins, as well as lengthy exposure times in vapor or liquid phases to deposit the self-assembled monolayer (SAM).[3, 4] These processes are generally not compatible with a roll-to-roll line without adding multiple, complex in-line processing steps and controlled environments. A simpler, roll-to-roll compatible method of reducing the surface energy of polymer resin molds would therefore be useful, if not required; especially for dense, high aspect ratio nanostructured resin molds.

Herein we describe a unique approach to surface chemistry modification of polymer resin molds through the introduction of multi-functional silicone roll-mounted stamps for UV roll-to-roll nanoimprinting, where the latter serves as both a patterning template as well as a release agent transfer vehicle. Sustained release agent transfer is achieved by taking advantage of a unique property of silicone solids to absorb significant quantities of similar, liquid oligomeric silicones due to entropy driven solubility.[27, 28] Low molecular weight
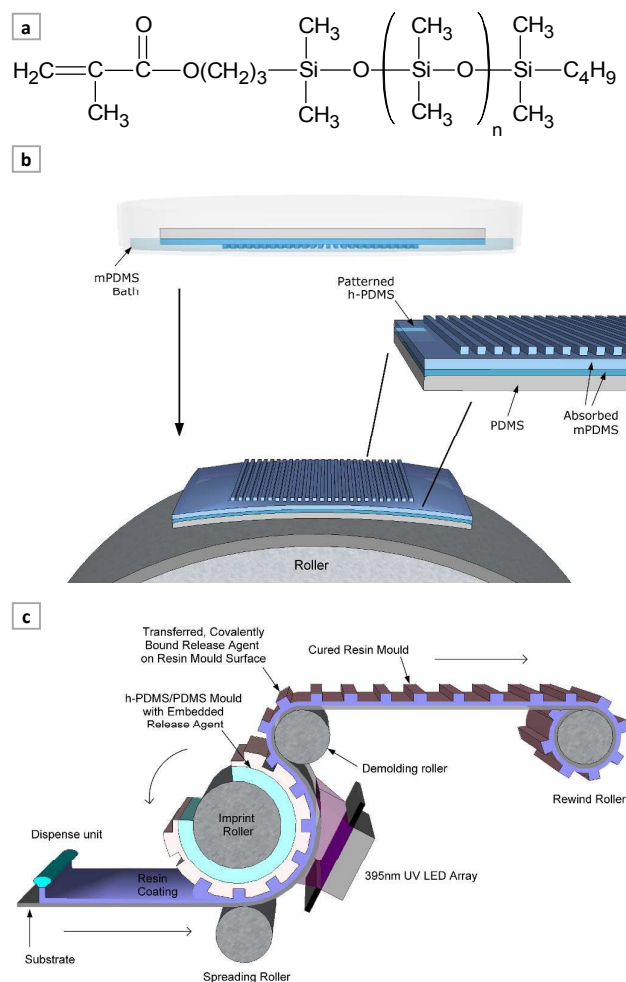

Fig. 1 (a) Chemical structure of asymmetric monomethacryloxypropyl-terminated polydimethylsiloxane (mPDMS). (b) Schematic of the mPDMS application approach to h-PDMS/PDMS stamps, the roll mounting strategy and zoomed view of the layer structure after mPDMS absorption. mPDMS is absorbed exclusively through the patterned face of the h-PDMS layer. (c) UV roll-to-roll nanoimprinting system schematic showing how the h-PDMS/PDMS stamp with embedded mPDMS is mounted on the imprint roller, allowing continuous transfer of mPDMS to fabricated resin molds.

methacrylated oligomeric silicones have very low surface tension, absorb quickly and spontaneously into silicone solids, and can serve as polymerizable release agent monomers in a UV-based nanoimprinting process. Here we show successful dissolution of monomethacryloxypropyl-terminated polydimethylsiloxane (mPDMS, MW 600-800, 6-9 mPa·s, see chemical structure and dissolution scheme in Fig. 1) in bi-layer silicone hard PDMS/PDMS (h-PDMS/PDMS) roll-mounted stamps, followed by transfer of the mPDMS to fabricated resin mold surfaces in a UV roll-to-roll nanoimprinting process for the purpose of controlling the resin mold surface energy.

mPDMS transfer is facilitated by ensuring that it is soluble in the liquid resin coating, such that contacting the h-PDMS/PDMS stamp with the liquid resin creates a spontaneous flux of mPDMS release agent across the h-PDMS/resin interface, as this increases the system

configurational entropy.[27] The objective is then to cure the resin coating by UV exposure with a maximum sustainable flux of release agent crossing this interface such that the release agent polymerizes at the formed resin mold surface. A release agent concentration gradient is then set up in the h-PDMS/PDMS stamp as it is removed from the h-PDMS surface layer over multiple roll-to-roll imprint cycles. This then leads to migration of additional release agent to the silicone stamp surface, enabling sustainable transfer to subsequent resin molds and a sustainable reduction in their surface energy. In summary, the main advantages of such an approach to surface energy reduction are: 1) no modifications required to the bulk chemistry of the resin mold, 2) no additional in-line processing steps are required, and 3) as this is a spontaneous process, the reduction in surface energy occurs automatically with the production of resin molds in the UV roll-to-roll nanoimprinting process.

Theoretical Background

To accomplish the task of dissolution of liquid oligomeric silicone into an intermediate roll-mountable solid silicone stamp without drastic swelling of the stamp features, h-PDMS/PDMS bi-layer silicone stamps were fabricated such that the stamp patterns were formed in a thin, heavily cross-linked h-PDMS layer backed by a soft, flexible PDMS base layer (see Supplementary Information, Table S2).[29, 30] Whereas Sylgard 184 PDMS generally obtains a Young's Modulus of ~2 MPa,[31] the most heavily crosslinked formulations of h-PDMS can achieve up to 9 MPa.[29]   The larger modulus overcomes many issues with monolithic Sylgard 184 PDMS stamps, such as poor mechanical stiffness, poor replication fidelity at high resolution, and feature collapse at higher aspect ratios. The two materials are often combined into a bi-layer composite stamp for use in soft lithography, which has been shown to achieve sub-40 nm feature resolution.[32]

An h-PDMS pattern-carrying layer was crucial in mitigating the swelling response of the h-PDMS/PDMS bi-layer roll-mounted stamp to mPDMS absorption. To be sure, h-PDMS still swells with mPDMS uptake, however h-PDMS was instrumental in keeping the degree of swelling relatively low while retaining adequate solubility with mPDMS. Other silicones such as Sylgard 184 PDMS are known to swell to such a large extent when absorbing good solvents that irreversible deformations can occur.[28] The swelling response of h-PDMS to good solvents is much smaller than conventional Sylgard 184 PDMS due to its crosslink density. For h-PDMS, the molar mass between crosslinks in the polymerized network, M_N of VDT-731 is 987 g mol^{-1}, while the molecular weight of a basic unit of dimethylsiloxane is 74, so the number of repeat units between crosslinks N_e is only ~13 – 14.[29] In contrast, M_N for Sylgard 184 is roughly double, at 1957 g mol^{-1} giving an N_e of ~26 – 27.[33] The increase in crosslink density will increase the thermodynamic barrier to mPDMS dissolution as given by the well-known Flory-Rehner model at equilibrium:[34, 35]

$$\frac{\partial}{\partial x_s}(\Delta G_{mix} + \Delta G_{elastic}) = 0 = ln(1 - v_N) + v_N + \chi v_N^2 + \frac{\rho_N V_s}{M_N}\left(v_N^{\frac{1}{3}} - \frac{v_N}{2}\right) \quad (1)$$

where x_s is the mole fraction of the permeate solvent (mPDMS), ΔG_{mix} is the free energy change upon mixing of a polymer and solvent, $\Delta G_{elastic}$ is the free energy change due to swelling of the polymer network, v_N is the volume fraction of the polymer in the swollen gel, $1/v_N$ is the swelling ratio, χ is the Flory-Huggins interaction parameter, ρ_N is the polymer density, M_N is the average chain molecular weight between crosslinks, ρ_N/M_c is the crosslink density of the polymer, and V_s is the molar volume of the solvent. The first three terms on the right hand side of Eqn. 1 take into consideration the free energy change due to mixing. The final term accounts for the negative entropy change due to swelling. It can be seen that the swelling term becomes large with the cross-link density, or as M_N becomes small. This will require v_N to approach 1 so that the free energy change of mixing terms will balance the swelling terms, and correspondingly the swelling ratio will also approach 1. Refinements to the Flory-Rehner model to more accurately predict the swelling behavior of highly crosslinked polymers where $N_e < 100$ were made by Kovac,[36] Lucht and Peppas.[37] However, at constant χ all three models predict a significant reduction in swelling with increasing ρ_N/M_c, which is sufficient for our purposes.

Separately, if a relatively high molar volume permeate is used then the swelling ratio required to balance Eqn. 1 will also be small. The proper derivation of the diffusion coefficient for the permeate-solid network pair depends on the unit chain length of the permeate. In the present work, mPDMS has a mean monomer chain length N ≈ 12. This is close to the entanglement length for h-PDMS (N_e ~ 13 - 14), but below the threshold where entanglement constraints will influence the motion of the permeate chains.[38] For cases where the permeate chain length is less than the entanglement length of the network, the Rouse model is appropriate.[39, 40] In the Rouse model the chain center of mass diffusion coefficient is given by the Einstein relation:

$$D_R = \frac{kT}{N\xi} \quad (2)$$

Where D_R is the diffusion coefficient, k is the Boltzmann constant, T is temperature, and ξ is the friction coefficient of the viscous medium experienced by each monomer of the permeate chain of N monomers. Here, the diffusion coefficient scales as N^{-1}.[41] Therefore it is important to minimize N (being proportional to the molar volume of the permeate) for the purpose of speeding up the infiltration dynamics to practical time scales.

For permeate chains whose length is significantly greater than the entanglement length of the solid network (there is disagreement over the precise threshold value, but N ≥ 2.5N_e is commonly cited),[38] reptation theory better approximates the motion of the permeate.[42, 43] The reptation-dominated self-diffusion coefficient exhibits an even greater dependency on N, scaling as N^{-2}.[43] Note that these scaling parameters are for self-diffusion in a polymer gel and assumes the permeate chain has precisely the same chemical composition as the host

network. Since mPDMS is chemically similar to the polysiloxane backbone of h-PDMS, but differs in molecular weight and the composition of its terminating groups, there is a thermodynamic acceleration of the inter-diffusion of the two species due to a negative ΔG_{mix} in addition to Brownian motion. Given the relatively low molecular weight of mPDMS, the acceleration arises principally from an increase in the combinatorial entropy on mixing,[44] where the free energy of mixing of a polymer-solvent system is given by the Flory-Huggins equation:

$$\Delta G_{mix} = RTV\left[\frac{\rho_s v_s}{M_s}\ln v_s + \frac{\rho_N v_N}{M_N}\ln v_N\right] + RTn_s v_N \chi \qquad (3)$$

where R is the gas constant, T is temperature, V is the total volume, ρ_s is the solvent permeate density, M_s is the molecular weight of the permeate, v_s is the volume fraction of the permeate, and n_s is the number of moles of permeate.[44] For a good solvent, χ is typically ~0.5 or less and the combinatorial entropy of mixing terms give $\Delta G_{mix} < 0$, with ΔG_{mix} becoming increasingly negative with smaller M_s. This thermodynamic acceleration will increase the diffusion scaling law by a factor of N. From this discussion, it can be concluded that the chain length N of the silicone permeate should be minimized in order to maximize the configurational entropy change upon mixing and maintain Rouse chain diffusion behavior within the host silicone solid. In addition, the crosslink density of the host silicone should be maximized (M_N, N_e minimized) in order to minimize the swelling ratio. Finally, these quantities must be balanced such that co-miscibility is maintained and the materials can be processed into a suitable stamp with embedded release agent.

Results & Discussion

500 nm diameter, aspect ratio 1 hexagonal pillar, and 500 nm half-pitch, aspect ratio 4 grating h-PDMS/PDMS stamps were obtained using reformulated h-PDMS as described above (see Table S1 for precise master mold geometries). In order to control the convexity of the h-PDMS/PDMS stamps, all such stamps were exposed to pure liquid mPDMS exclusively through the h-PDMS pattern-carrying face for a period of 3 minutes (see Fig. 1b), which was determined empirically through high resolution video as the time where a 2.5 x 2.5 x 0.3 cm bi-layer stamp begins to visibly curl with the pattern-carrying face bending slightly outward in a convex manner. This serves as a visual indication that the mPDMS has fully wet the h-PDMS layer and is proceeding to swell the PDMS backing. Recommended mPDMS exposure time will of course vary according to the h-PDMS layer thickness (~10 μm in the present work). Mild curling was removed with tension during wrap mounting onto the imprint roller of our UV roll-to-roll nanoimprinting apparatus.

h-PDMS/PDMS bi-layer stamps with embedded mPDMS were thus integrated into the UV roll-to-roll nanoimprinting scheme for resin mold fabrication shown in Fig. 1c. The process involves an unwind stage for the flexible substrate web line, continuous inkjet dispensing of resin onto the h-PDMS/PDMS roll-mounted stamp, stack formation with a spreading roller where the inkjet dispensed drop curtain is spread against the web to form a coating, curing of the resin coating against the h-PDMS/PDMS stamp by 395 nm UV LED irradiation through the web, followed by separation and rewinding of the finished resin mold reel. The h-PDMS/PDMS stamp was mounted onto the imprint roller of our UV roll-to-roll nanoimprinting apparatus as shown in Fig. 2a. Our apparatus is capable of mounting multiple discrete sheet molds that are shorter than the total circumference of the imprint roller. Further details on our roll-to-roll nanoimprinting system can be found elsewhere.[14]
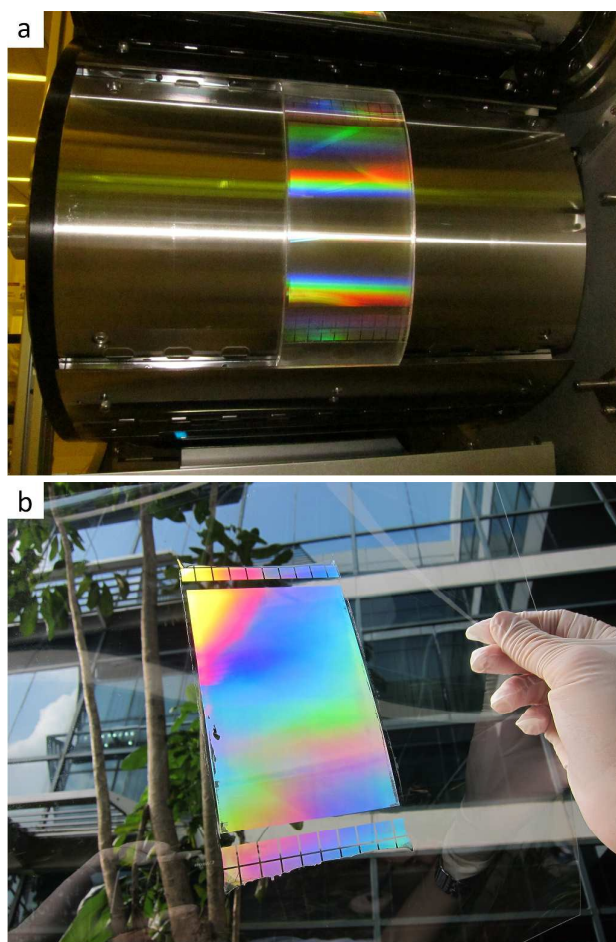
Fig. 2 (a) Large area 160 x 75 x 4 mm, 500 nm diameter aspect ratio 1 hole, h-PDMS/PDMS composite stamp mounted in our UV roll-to-roll nanoimprinting system, post-mPDMS exposure, after an initial imprint cycle to remove residual surface mPDMS. (b) corresponding resin mold fabricated via UV roll-to-roll nanoimprinting with transferred surface mPDMS.

In terms of resin selection for fabrication of resin molds, a test bed resin comprised of 59% wt. 1,6 hexanediol diacrylate monomer, 39% wt. neopentyl glycol diacrylate crosslinker, and 2% wt. 4,4'-bis(diethylamino)benzophenone photoinitiator was formulated. The mixture has a low viscosity of ~9 mPa·s for compatibility with inkjet dispense, which is the mode of

Materials Horizons

COMMUNICATION

resin deposition used by our UV roll-to-roll nanoimprinting system. The resin components were selected to be silicon-free for the purpose of later detection of transferred mPDMS via XPS characterization. mPDMS is also miscible in the chosen formulation and testing in our lab has shown that phase segregation does not occur on polymerization in thin film form until the concentration exceeds 4% wt. Spontaneous diffusion of highly soluble solvents out of swollen silicone solids into less-soluble solvent immersions is well documented experimentally, so long as both solvents are miscible in each other.[28] From thermodynamics, this occurs because the resin host liquid is not cross-linked and therefore the system configurational entropy will further increase with diffusion and mixing of mPDMS upon contact with a resin coating (assuming predominantly dispersive intermolecular interactions, i.e. no overriding positive enthalpy contribution to the free energy change). The present method to lower replicated resin mold surface energy thus relies entirely on spontaneous entropy-driven processes.

Demonstration of large area fabrication against h-PDMS/PDMS stamps with embedded mPDMS was accomplished with a 160 x 75 mm, 500 nm diameter, aspect ratio 1 hexagonal pillar array stamp, with the fabricated resin mold result shown in Fig. 2b. Separation of the resin mold was greatly assisted by the use of 395 nm UV LED exposure to cure the resin, as the narrow-band emission of the LED array ensured that the mPDMS did not self-polymerize in the bulk of h-PDMS/PDMS stamp, leading to significant polymerization across the h-PDMS/resin interface and locking the imprint stack together. Early test results in batch mode indicated that mPDMS will self-polymerize in this manner with mercury-arc lamp illumination due to 200 - 254 nm emission present in the lamp spectrum.[45-47]

Contact angle measurements in concert with XPS measurements were used to characterize the degree of mPDMS release agent transfer from h-PDMS/PDMS silicone roll-mounted sheets to blank (flat, featureless) cured resin mold surfaces, transfer sustainability over 20 imprint cycles, and the increase in hydrophobicity over reference samples. For these experiments, the native un-crosslinked dimethylsiloxane oligomers present in the h-PDMS/PDMS silicone sheets were extracted with solvents. Here it must be noted that highly soluble solvents such as diisopropylamine, triethylamine and hexanes could not be used to extract un-crosslinked oligomers from h-PDMS/PDMS composite sheets due to swelling mismatch. Because these solvents cause such dramatic swelling of PDMS, with swelling ratios in the range of ~1.3 − 2.13,[28] the mismatch stress with h-PDMS becomes so great that the h-PDMS fails due to cracking. Thus, lower solubility solvents were used to extract the h-PDMS/PDMS sheets such that while the native un-crosslinked oligomers were not completely removed from the h-PDMS surface, their concentration was greatly reduced relative to the amount of mPDMS release agent introduced to the h-PDMS/PDMS sheets (see Supporting Information).

The surface energy of all sequentially imprinted blank resin mold samples and reference samples were obtained by static solid-air-liquid contact angle goniometry, using the Owens-Wendt method with water and diiodomethane as the polar and dispersive test liquids, respectively.[48] Fig. 3 shows the total surface energy of sequentially imprinted blank resin molds, where the error bars represent the standard deviation for N = 5 measurements per sample per test liquid. For comparison, a second series of 20 roll-to-roll nanoimprinted blank resin molds was also analyzed where the h-PDMS/PDMS sheet was substituted for a thin sheet of flexible glass with physisorbed mPDMS, where the glass was treated with an h-PDMS pre-polymer mixture via spincoating, which was then subsequently removed prior to gelling with hexanes in an ultrasonic bath. This gave the effect of a h-PDMS surface without the capacity to absorb any significant quantity of mPDMS into the material bulk. This serves as a useful reference for isolating the presence of a release agent flux across the h-PDMS/resin coating interface and migration of mPDMS release agent from the bulk h-PDMS/PDMS sheet to this interface (i.e. the presence of an active reservoir of release
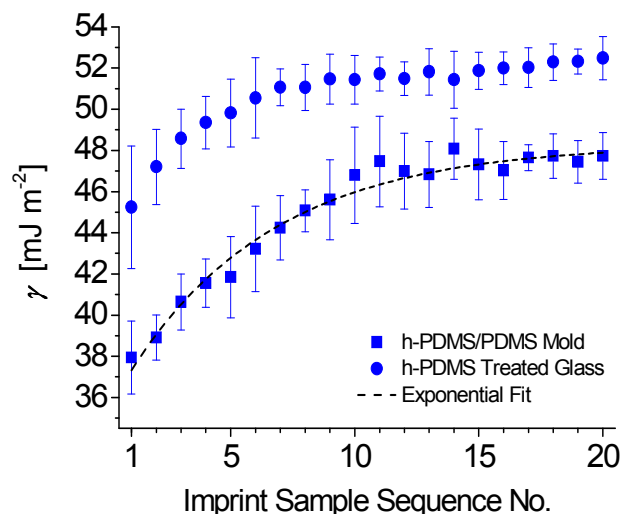

Fig. 3 Plot of the total surface energy (γ), calculated by the Owens-Wendt method, of sequentially imprinted blank resin molds cured against extracted bi-layer h-PDMS/PDMS sheets with embedded mPDMS (squares), as well as against h-PDMS treated glass that had been immersed in liquid mPDMS (circles). The former series was fit to a first-order exponential function with adjusted R-squared of 0.98 of the form $y = Ae^{-x/\lambda} + y_o$, where A=-13.05, λ=5.82, and y_o=48.31. Error bars show the standard deviation calculated from N=5 measurements per sample per test liquid.

agent embedded in the silicone mold) through its contrasting effect on the output resin mold surface energy. The lowest mean recorded surface energy was recorded for the first sample cured against an h-PDMS/PDMS sheet with embedded release agent at 38 mJ m^{-2}, whereas the reference counterpart was measured at ~45 mJ m^{-2}. Approximately the next 10 samples record an upward sloping trend in surface energy, stabilizing at about 47 mJ m^{-2} for the bi-layer silicone sheet case. The h-PDMS treated glass series also trends upward in surface energy however it maintains a 5-7 mJ m^{-2} gap with the h-PDMS/PDMS sheet series, indicating that the h-PDMS/PDMS sheet case benefits from a release agent flux across the h-

COMMUNICATION

PDMS/resin interface, leading to an increase in surface mPDMS concentration on the resin mold. If this were not the case, it was expected the two data sets would eventually coincide as surface mPDMS is removed.

The leveling off of the h-PDMS/PDMS trend after about the 10th sample also indicates migration of mPDMS release agent from the bulk h-PDMS / PDMS sheet to the h-PDMS/resin coating interface to stabilize transfer. A first-order exponential fit to the h-PDMS/PDMS sheet data extrapolates a stable surface energy of ~47 mJ m^{-2} with an adjusted R-square of 0.98. An additional silicone-free reference, where the blank resin mold is cured against a flat (featureless) nickel shim, was recorded at 55 mJ m^{-2} (SD ± 1, see Table S1). This indicates that mPDMS transfer can sustainably reduce the surface energy of our blank resin mold by ~8 mJ m^{-2} at 1 m min^{-1} (approx. 1 sample min^{-1}) throughput. For comparison, mPDMS transfer from h-PDMS treated glass leveled off at a higher

sample sets as above was utilized. Fig. 4 shows the trend of silicon (Si) atomic concentration at the surface of blank resin molds with increasing sample count, which is proportional to mPDMS surface concentration. The solvent-extracted h-PDMS/PDMS mold with embedded mPDMS series clearly exhibits a shallower initial downward slope in comparison with mPDMS transferred from h-PDMS treated glass. Along with the consistent improvement in transferred Si, the shallower initial downslope and subsequent leveling off after ~11 imprint cycles also indicates that mPDMS is migrating to the h-PDMS/resin interface and producing a flux across the interface into the liquid resin prior to UV curing. If additional mPDMS reaches the h-PDMS/resin interface, the loss rate of transferred mPDMS will decrease with subsequent samples relative to the h-PDMS treated glass case as shown, where for the latter case mPDMS is only physisorbed at the surface and migration from the bulk
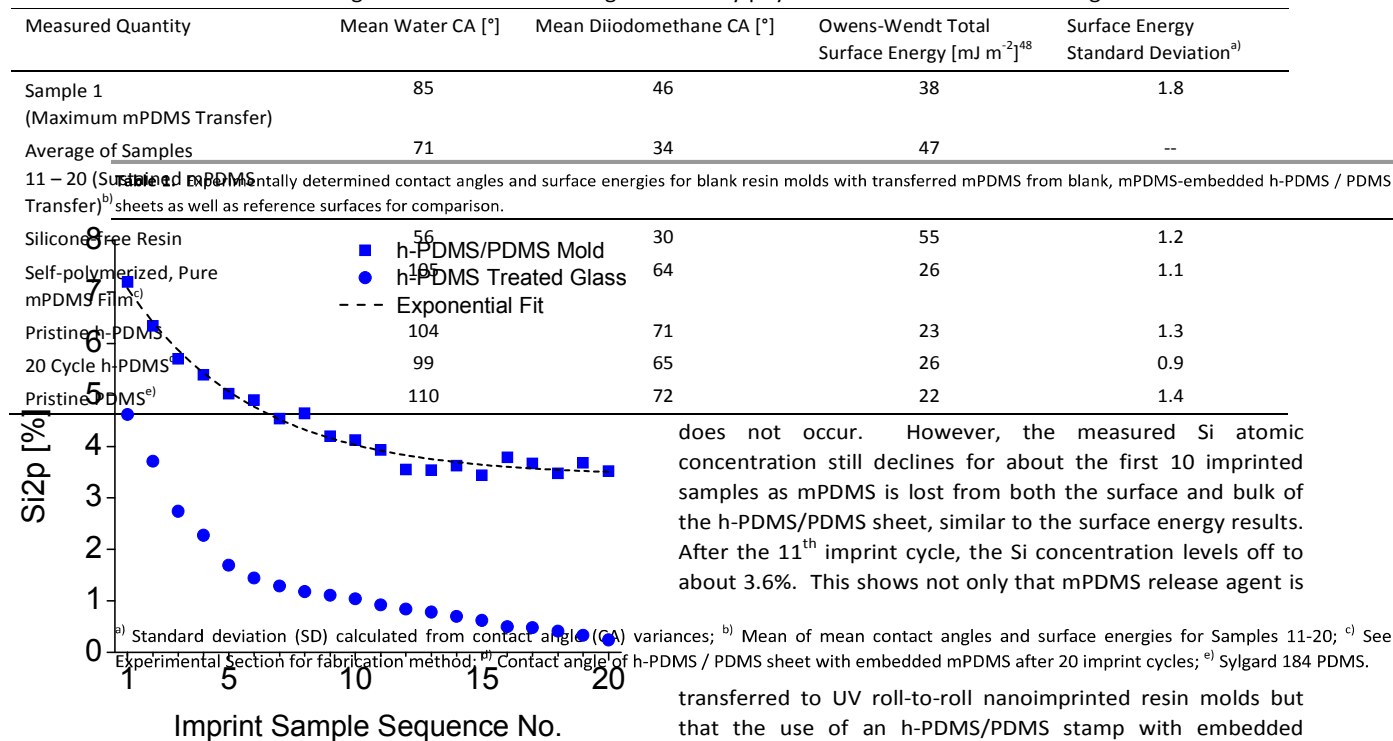
Measured Quantity	Mean Water CA [°]	Mean Diiodomethane CA [°]	Owens-Wendt Total Surface Energy [mJ m^{-2}][48]	Surface Energy Standard Deviation[a)]
Sample 1 (Maximum mPDMS Transfer)	85	46	38	1.8
Average of Samples 11 – 20 (Sustained mPDMS Transfer)[b)]	71	34	47	--
Silicone-Free Resin	56	30	55	1.2
Self-polymerized, Pure mPDMS Film[c)]	105	64	26	1.1
Pristine h-PDMS	104	71	23	1.3
20 Cycle h-PDMS	99	65	26	0.9
Pristine PDMS[e)]	110	72	22	1.4

Table 1. Experimentally determined contact angles and surface energies for blank resin molds with transferred mPDMS from blank, mPDMS-embedded h-PDMS / PDMS sheets as well as reference surfaces for comparison.

does not occur. However, the measured Si atomic concentration still declines for about the first 10 imprinted samples as mPDMS is lost from both the surface and bulk of the h-PDMS/PDMS sheet, similar to the surface energy results. After the 11th imprint cycle, the Si concentration levels off to about 3.6%. This shows not only that mPDMS release agent is

a) Standard deviation (SD) calculated from contact angle (CA) variances; b) Mean of mean contact angles and surface energies for Samples 11-20; c) See Experimental Section for fabrication method; d) Contact angle of h-PDMS / PDMS sheet with embedded mPDMS after 20 imprint cycles; e) Sylgard 184 PDMS.

Fig. 4 Plot of the surface silicon atomic concentration (Si2p peak, ~102 eV), as measured by XPS for sequentially imprinted blank resin molds cured against extracted bi-layer h-PDMS/PDMS sheets with embedded mPDMS (squares), as well as against h-PDMS treated glass that had been immersed in liquid mPDMS (circles). The former series was fit to a first-order exponential function with adjusted R-squared of 0.98 of the form $y = Ae^{-x/\lambda} + y_o$, where A=4.46, λ=5.02, and y_o=3.42.

surface energy of about 51 mJ m^{-2} after sample 6, with the average measured surface energy continuing on a gradual slope higher with subsequent samples toward the silicone-free surface energy. This secondary slope can be attributed to radical scission and mechanical removal of surface h-PDMS chains, similar to what has been recorded for other anti-stick coating treatments.[13]

To further confirm sustainable transfer of mPDMS to blank resin molds, XPS analysis of neighboring areas of the same 20

transferred to UV roll-to-roll nanoimprinted resin molds but that the use of an h-PDMS/PDMS stamp with embedded mPDMS enables sustained transfer of mPDMS to resin mold surfaces. Again, an exponential decay fit to the data extrapolates a stabilized Si concentration beyond 20 samples of 3.4% with an adjusted R-square of 0.98. Finally, for the h-PDMS treated glass case, the loss of h-PDMS chains is shown clearly after surface mPDMS is removed from the 6th sample onwards, in agreement with the secondary slope interpretation of the surface energy results. XPS confirmation was useful here as the surface energy measurements were not sensitive enough to fully resolve the secondary slope in the h-PDMS treated glass case above the noise level defined by the standard deviation (Fig. 3 error bars). By the 20th sample, the Si surface concentration is negligible.

A helpful summary of experimentally determined quantities is provided in Table 1. Contact angle data as well as

       COMMUNICATION

total surface energy results are provided for blank resin molds with transferred mPDMS from mPDMS-embedded h-PDMS/PDMS sheets as in Fig. 3, as well as reference surfaces for comparison. The data presented shows that the maximum surface energy reduction achieved was ~17 mJ m^{-2} relative to silicone-free blank resin molds cured against flat nickel shims. The maximum possible surface energy reduction achievable is ~29 mJ m^{-2} with respect to pure, self-polymerized mPDMS films. The pure mPDMS film surface energy of ~26 mJ m^{-2} was similar to that recorded for h-PDMS/PDMS sheets with embedded mPDMS after 20 imprint cycles, though the latter is a combination of surface mPDMS, h-PDMS and residual organics from the resin and therefore the similarity is likely coincidental. However, the 20th imprint cycle result helps to confirm that resin organics are not caking onto the h-PDMS/PDMS sheet surface to a noticeable extent. Finally, pristine h-PDMS and PDMS contact angle and surface energy measurements are provided for comparison to the other results obtained as well as similar measurements in the

expansion of line cavities is visually observable. Quantification of these dimensional changes is provided in Table 2 in the form of percentage changes in length of the measured dimension with respect to the equivalent master mold dimension. For reverse-tone measurements, such as the fabrication of an h-PDMS/PDMS stamp against a silicon master, the change in the opposing dimension is given (for example, the line width of the silicon master was compared to the line cavity width in h-PDMS to calculate the dimensional change, e.g. 2.1%). This allows a given feature dimension on the master to be followed out to the resin mold fabrication step, which has the same tone as the master. The acrylate resin shrinkage of 2.5 – 2.8% was determined by performing a batch UV-NIL process with the resin against the silicon master directly and measuring the dimensional changes. Finally, the variation in line height was doubled for consistency with line width measurements which capture the dimensional change from both ends of the feature.

The observed absolute dimensional variations for the h-PDMS curing step (1.8 – 2.1%), as part of the h-PDMS/PDMS
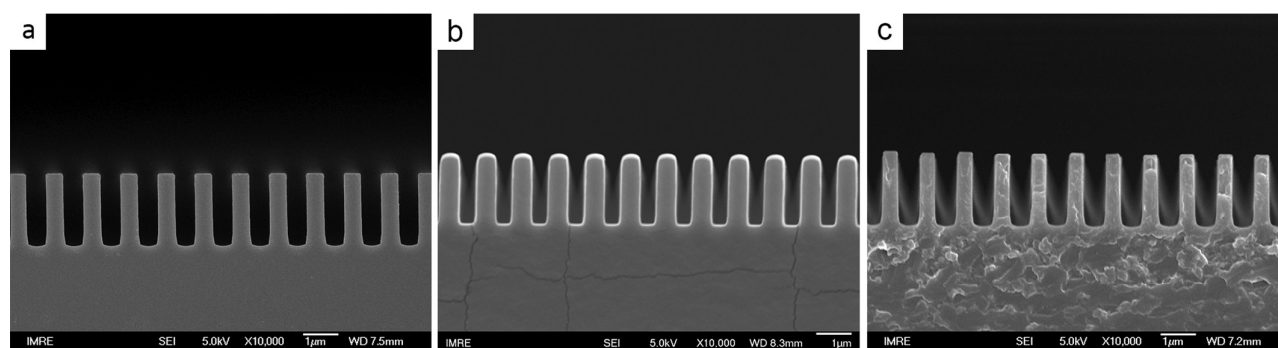

Fig. 5 Representative SEM cross-section images of 500 nm half-pitch, aspect ratio 4 grating molds following the fabrication process from (a) the silicon master, (b) an h-PDMS / PDMS stamp replicated from the Si master (patterned h-PDMS layer shown) prior to mPDMS exposure, (c) a UV roll-to-roll nanoimprinted resin mold with transferred mPDMS fabricated against the aforementioned h-PDMS / PDMS stamp.

literature.

While the h-PDMS layer of h-PDMS/PDMS bi-layer silicone stamps has a reduced swelling ratio compared to Sylgard 184 PDMS, h-PDMS does undergo some swelling upon absorption of mPDMS. In addition, the acrylate resin formulation used will also shrink upon polymerization. Dimensional variation of 500 nm half-pitch, aspect ratio 4 grating structures was investigated by cross-sectional field-emission scanning electron microscopy (FESEM) through the entire fabrication sequence from the silicon master to the h-PDMS/PDMS intermediate stamp (prior to liquid mPDMS exposure) and finally the UV roll-to-roll nanoimprinted resin mold (Fig. 5). The effect of mPDMS swelling can then be inferred from these

stamp fabrication, were consistent with literature values for linear shrinkage of h-PDMS (1.6 ±0.5%).[49] As for the resin mold fabricated with transferred mPDMS, the absolute dimensional changes varied from 4.3 to 9.8%. This is the combined dimensional change produced by the entire fabrication process. In particular, the line height increased as a result of the effect of mPDMS swelling, while the line width shrank, causing an increase in the grating aspect ratio from ~4.3 to ~4.8. This is a very interesting effect as there are very few, if any, techniques that can replicate an existing feature set and then incorporate an increase to the aspect ratio of that set. Moreover, the aspect ratio increase was accomplished in part by an increase in the line height, which is especially

	Change in Line Width (%)	Change in Line Cavity Width (%)	Change in Line Height (%)[a]
h-PDMS/PDMS Stamp[b]	2.1	-1.8	-1.8
Acrylate Resin[c]	-2.5	1.6	-2.8
Fabricated Resin Mold w/ Transferred mPDMS	-9.8	8.3	4.3
mPDMS Absorption[d]	-9.4	8.6	9.0

measurements since mPDMS is slightly volatile and is incompatible with a high-vacuum SEM chamber.

Comparing the silicon master (Fig. 5a) with the fabricated resin mold (Fig. 5c), shrinkage of the fabricated lines and

unique. This occurred in spite of line height losses introduced by h-PDMS and acrylate resin curing shrinkages. In contrast, the aforementioned shrinkages led to offsetting changes in line width and line cavity width upon fabrication of the resin

Positive values indicate expansion while negative values indicate shrinkage. a) Measured variations were doubled for consistency with width measurements (see text); b) Features were fabricated in h-PDMS. As this is a reverse-tone replica of the master, the change in the opposing dimension relative to the master mold is given.; c) Batch UV-NIL process (resin 5000 nm) inferred from a direct measurement of all other dimensional changes in the process, following contact with the acrylate resin for 1 minute.

mold, which led to a larger overall variation in line width and line cavity width. Direct measurement of all other dimensional changes allows the dimensional change caused by swelling due to mPDMS absorption to be backed out. In absolute terms the swelling effect caused dimensional variation ranging from 8.6 to 9.4%. While comparatively large relative to ordinary curing shrinkage values, the swelling effect was still sufficiently small such that major deformations in feature shape or contour were not observed beyond linear changes in feature width, height and aspect ratio. A positive increase in feature height of 9% induced by mPDMS swelling could furthermore be viewed as a desirable characteristic and closer study would be worthwhile to see if the effect can be magnified.

Conclusions

The present work introduces a unique method of transferring methacrylated, silicone-based release agent molecules onto cured resin surfaces via UV roll-to-roll nanoimprinting as a means of reducing the surface energy of resin molds during fabrication without adding additional processing steps in-line. In particular, dissolution of mPDMS into bi-layer h-PDMS/PDMS silicone roll-to-roll compatible stamps is unique in that the stamp plays a dual role as both a lithographic template as well as a release agent transfer vehicle. This study is thus an early inquiry into multi-layer, roll-to-roll compatible silicone stamps with multiple process functions. Additionally, the reactive nature of mPDMS monomers allows participation in the resin polymerization reaction such that the mPDMS will become part of the polymerized network at the surface of the resin mold upon transfer from the silicone roll stamp. This approach thus reduces the surface energy without modifying the bulk chemistry of the resin, allowing the bulk resin formulation to be selected for application-specific properties such as high stiffness, hardness, scratch resistance and transparency.

There are additionally, multiple avenues for further performance improvement. First, since mPDMS is progressively lost while the embedded h-PDMS/PDMS stamp is held in contact with the liquid resin coating during the UV roll-to-roll nanoimprinting process, significant improvements in performance and sustainability could be realized by minimizing the contact time, which can be accomplished by simply increasing the throughput. In the present study, it is expected that most of the near-surface mPDMS embedded in the h-PDMS layer is lost during the first few imprint cycles as contact with the liquid resin coating is lengthy at ~1 minute per cycle. The near-surface mPDMS of a newly processed h-PDMS/PDMS stamp creates a steep concentration gradient against the release-agent free resin coating, and hence a maximized release agent flux across the h-PDMS/resin interface. At high throughput, where the contact time is a few seconds or less, more of the near-surface mPDMS embedded in the h-PDMS layer can be captured at the surface of polymerized resin molds. Moreover, the surface concentration of mPDMS should be significantly greater with the larger flux. The challenge would then be to maximize the release agent flux across the h-

PDMS/resin interface without exceeding the release agent migration rate to the h-PDMS surface, or else implement a release agent deposition and absorption step to the silicone mold in-line to maintain a large flux back into the resin coating.

A significantly higher molecular weight acrylate resin formulation, or one with more polar (insoluble) components, would also help prevent the h-PDMS/PDMS stamp from absorbing those resin components that could polymerize into the h-PDMS bulk over a large number of imprint cycles and gradually form a diffusion barrier to mPDMS. This was not directly observed over 20 imprint cycles in the present study, as the photoinitiator used in the acrylate resin formulation is not soluble in silicones at 1 – 2% wt. concentrations typical for UV curing and long-wavelength UV exposure precludes self-polymerization of embedded acrylates. However, gradual polymerization into the h-PDMS bulk over a much larger number of imprint cycles would not be surprising.

Various improvements to the process chemistry could also be implemented. For example, an even lower molecular weight oligomeric silicone release agent would tend to have lower surface tension as well as faster diffusion dynamics that could enable greater amounts of sustained transfer to resin mold surfaces at higher throughput. Furthermore, adding fluorinated groups to the silicone release agent would improve both its hydrophobicity and oleophobicity relative to mPDMS. This could allow the release agent to have a lower surface tension than the surface energy of pristine h-PDMS, which would accelerate surface migration with successive resin mold fabrication cycles thanks to a negative enthalpy contribution in addition to the potential increase in entropy provided by the concentration gradient that would form at the h-PDMS surface. However, the addition of fluorine groups would come at the expense of solubility in h-PDMS. Migrating the entire network-permeate system to fluorosilicone elastomers with reactive fluorosilicone release agent monomers might therefore be a worthwhile alternative system to study.

Acknowledgements

References

1   L. J. Guo, *J. Phys. D: Appl. Phys.*, 2004, **37**, R123.
2   J. J. Dumond and H. Y. Low, *J. Vac. Sci. Technol., B*, 2012, **30**, 010801-010828.
3   M. Beck, M. Graczyk, I. Maximov, E. L. Sarwe, T. G. I. Ling, M. Keil and L. Montelius, *Microelectron. Eng.*, 2002, **61– 62**, 441-448.
4   S. Garidel, M. Zelsmann, P. Voisin, N. Rochat and P. Michallon, presented in part at the Proc. SPIE 6517, Emerging Lithographic Technologies XI, San Jose, CA, February, 2007.

5   D. Y. Khang and H. H. Lee, *Langmuir*, 2004, **20**, 2445-2448.
6   D. R. Barbero, M. S. M. Saifullah, P. Hoffmann, H. J. Mathieu, D. Anderson, G. A. C. Jones, M. E. Welland and U. Steiner, *Adv. Funct. Mater.*, 2007, **17**, 2419-2425.
7   J. P. Rolland, E. C. Hagberg, G. M. Denison, K. R. Carter and J. M. DeSimone, *Angewandte Chemie-International Edition*, 2004, **43**, 5796-5799.
8   S. S. Williams, S. Retterer, R. Lopez, R. Ruiz, E. T. Samulski and J. M. DeSimone, *Nano Lett.*, 2010, **10**, 1421-1428.
9   M. Bender, U. Plachetka, J. Ran, A. Fuchs, B. Vratzov, H. Kurz, T. Glinsner and F. Lindner, *J. Vac. Sci. Technol., B*, 2004, **22**, 3229.
10   S. H. Ahn and L. J. Guo, *Adv. Mater.*, 2008, **20**, 2044-2049.
11   S. H. Ahn and L. J. Guo, *ACS Nano*, 2009, **3**, 2304-2310.
12   W. B. Jackson, C. Perlov, M. Amanza-Workman, S. Braymen, A. Chaiken, F. Jeffrey, J. Hauschildt, A. Jeans, O. Kwon, H. Luo, P. Mei and C. Taussig, presented in part at the 2007 Digest of the Leos Summer Topical Meetings, New York, 2007.
13   D. Truffier-Boutry, M. Zelsmann, J. De Girolamo, J. Boussey, C. Lombard and B. Pépin-Donat, *Appl. Phys. Lett.*, 2009, **94**, 044110.
14   J. D. Jarrett, M. Kambiz Ansari, Y. Yew Sok, T. Christina, F. Jerry Ying Hsi, L. Heow Pueh and L. Hong Yee, *Nanotechnology*, 2012, **23**, 485310.
15   D. Matsukawa, H. Wakayama, K. Mitsukura, H. Okamura, Y. Hirai and M. Shirai, presented in part at the Proc. SPIE 7273, Advances in Resist Materials and Processing Technology XXVI, San Jose, CA, USA, 2009.
16   D. Matsukawa, H. Okamura and M. Shirai, *J. Photopolym. Sci. Technol.*, 2010, **23**, 781-787.
17   H. Shinohara, T. Tashiro, T. Ookawa and H. Nishihara, *IEEJ Transactions on Sensors and Micromachines*, 2012, **132**, 235-239.
18   Y. Engel, J. D. Schiffman, J. M. Goddard and V. M. Rotello, *Mater. Today*, 2012, **15**, 478-485.
19   L. J. Guo, X. Cheng and C. F. Chou, *Nano Lett.*, 2004, **4**, 69-73.
20   J. D. Hoff, L. J. Cheng, E. Meyhofer, L. J. Guo and A. J. Hunt, *Nano Lett.*, 2004, **4**, 853-857.
21   H. Shinohara, S. Fujiwara, T. Tashiro, H. Kitahara and H. Goto, *J. Photopolym. Sci. Technol.*, 2013, **26**, 113-117.
22   H. Chen, Q. Zhang and S. Y. Chou, *Nanotechnology*, 2015, **26**.
23   J. Frischeisen, Q. Niu, A. Abdellah, J. B. Kinzel, R. Gehlhaar, G. Scarpa, C. Adachi, P. Lugli and W. Bruetting, *Opt. Express*, 2011, **19**, A7-A19.
24   A. Y. Y. Ho, E. L. Van, C. T. Lim, S. Natarajan, N. Elmouelhi, H. Y. Low, M. Vyakarnam, K. Cooper and I. Rodriguez, *J. Polym. Sci., Part B: Polym. Phys.*, 2014, **52**, 603-609.
25   S.-H. Lee, K.-S. Han, J.-H. Shin, S.-Y. Hwang and H. Lee, *Prog. Photovoltaics Res. Appl.*, 2013, **21**, 1056-1062.
26   A. M. Almanza-Workman, C. P. Taussig, A. H. Jeans and R. L. Cobene, *J. Mater. Chem.*, 2011, **21**, 14185-14192.
27   C. S. Brazel and S. L. Rosen, *Fundamental Principles of Polymeric Materials*, Wiley, Hoboken, NJ, 2012.
28   J. N. Lee, C. Park and G. M. Whitesides, *Anal. Chem.*, 2003, **75**, 6544-6554.
29   H. Schmid and B. Michel, *Macromolecules*, 2000, **33**, 3042-3049.
30   T. W. Odom, J. C. Love, D. B. Wolfe, K. E. Paul and G. M. Whitesides, *Langmuir*, 2002, **18**, 5314-5320.
31   I. D. Johnston, D. K. McCluskey, C. K. L. Tan and M. C. Tracey, *J. Micromech. Microeng.*, 2014, **24**, 035017.
32   K. Hyewon, L. Jiyeon, P. Joonhyung and H. L. Hong, *Nanotechnology*, 2006, **17**, 197.
33   H. Yang, H. Wang, Z. Hou, P. Wang, B. Li, J. Li and J. Hu, *J. Mater. Chem.*, 2011, **21**, 4279-4285.
34   P. J. Flory and J. Rehner, *The Journal of Chemical Physics*, 1943, **11**, 521-526.
35   P. J. Flory, *The Journal of Chemical Physics*, 1950, **18**, 108-111.
36   J. Kovac, *Macromolecules*, 1978, **11**, 362-365.
37   L. M. Lucht and N. A. Peppas, *AIP Conference Proceedings*, 1981, **70**, 28-48.
38   D. Richter, L. Willner, A. Zirkel, B. Farago, L. J. Fetters and J. S. Huang, *Macromolecules*, 1994, **27**, 7437-7446.
39   P. E. Rouse, *J. Chem. Phys.*, 1953, **21**, 1272-1280.
40   M. Doi and S. F. Edwards, *The Theory of Polymer Dynamics*, Clarendon Press, Oxford, United Kingdom, 1988.
41   V. A. Harmandaris, V. G. Mavrantzas, D. N. Theodorou, M. Kröger, J. Ramírez, H. C. Öttinger and D. Vlassopoulos, *Macromolecules*, 2003, **36**, 1376-1387.
42   P. G. De Gennes, *Phys. Today*, 1983, **36**, 33-47.
43   P. G. de Gennes, *J. Chem. Phys.*, 1971, **55**, 572-579.
44   L. M. Robeson, *Polymer Blends: A Comprehensive Review*, Carl Hanser Verlag GmbH & Co. KG Munich, Germany, 2007.
45   F. Bauer, U. Decker, S. Naumov and C. Riedel, *Prog. Org. Coat.*, 2014, **77**, 1085-1094.
46   T. Scherzer, *Macromol. Chem. Phys.*, 2012, **213**, 324-334.
47   T. Scherzer, O. Savchuk, S. Naumov, W. Knolle and K. Heymann, *RadTech Report*, 2012, **4**, 18.
48   D. K. Owens and R. C. Wendt, *J. Appl. Polym. Sci.*, 1969, **13**, 1741-1747.
49   K. M. Choi and J. A. Rogers, *J. Am. Chem. Soc.*, 2003, **125**, 4060-4061.

A novel bi-layer silicone nanoimprint mold capable of dual-functionality as both a lithographic template and a release agent transfer vehicle.